



HAL
open science

Chemical transport-based growth of Si and SiGe nanowires

Ke Yang, Xianjun Zhu, Ruiling Gong, Ileana Florea, Pere Roca i Cabarrocas, Wanghua Chen

► **To cite this version:**

Ke Yang, Xianjun Zhu, Ruiling Gong, Ileana Florea, Pere Roca i Cabarrocas, et al.. Chemical transport-based growth of Si and SiGe nanowires. *Journal of Applied Physics*, 2025, 137 (4), 10.1063/5.0249864 . hal-04918468

HAL Id: hal-04918468

<https://cnrs.hal.science/hal-04918468v1>

Submitted on 29 Jan 2025

HAL is a multi-disciplinary open access archive for the deposit and dissemination of scientific research documents, whether they are published or not. The documents may come from teaching and research institutions in France or abroad, or from public or private research centers.

L'archive ouverte pluridisciplinaire **HAL**, est destinée au dépôt et à la diffusion de documents scientifiques de niveau recherche, publiés ou non, émanant des établissements d'enseignement et de recherche français ou étrangers, des laboratoires publics ou privés.



Distributed under a Creative Commons Attribution 4.0 International License

RESEARCH ARTICLE | JANUARY 28 2025

Chemical transport-based growth of Si and SiGe nanowires

Ke Yang ; Xianjun Zhu; Ruiling Gong; Ileana Florea ; Pere Roca i Cabarrocas ; Wanghua Chen  



J. Appl. Phys. 137, 044301 (2025)

<https://doi.org/10.1063/5.0249864>



Articles You May Be Interested In

KoopmanLab: Machine learning for solving complex physics equations

APL Mach. Learn. (September 2023)

Experimental realization of a quantum classification: Bell state measurement via machine learning

APL Mach. Learn. (September 2023)



Journal of Applied Physics

Special Topics Open
for Submissions

[Learn More](#)

Chemical transport-based growth of Si and SiGe nanowires

Cite as: J. Appl. Phys. 137, 044301 (2025); doi: 10.1063/5.0249864

Submitted: 20 November 2024 · Accepted: 5 January 2025 ·

Published Online: 28 January 2025



Ke Yang,¹  Xianjun Zhu,¹ Ruiling Gong,¹ Ileana Florea,^{2,3}  Pere Roca i Cabarrocas,²  and Wanghua Chen^{1,a)} 

AFFILIATIONS

¹School of Physical Science and Technology, Ningbo University, Ningbo 315211, China

²LPICM, CNRS, Ecole Polytechnique, Institut Polytechnique de Paris, 91128 Palaiseau, France

³Université Côte d'Azur (Unica), CNRS, CRHEA, 06905 Sophia Antipolis Cedex, France

^{a)}Author to whom correspondence should be addressed: chenwanghua@nbu.edu.cn

ABSTRACT

This study investigates the chemical transport-based growth of Si and Ge nanowires (NWs) using plasma-enhanced chemical vapor deposition. We found that Si NW growth requires a high etching temperature of 400 °C, related to a stronger Si–H bond energy compared to the Ge–H bond energy, allowing Ge NWs to form at 250 °C. The growth process is influenced by various parameters, including etching temperature, radio frequency power, GeH₄/SiH₄ precursor gas ratios, doping, and inter-electrode distance. Optimal Si NW growth is achieved at a substrate temperature of 250 °C during pre-coating and 400 °C during etching, with an RF power of 100 W. Conversely, Ge NWs can be fabricated at 250 °C, although they tend to be smaller and less dense. The study also highlights the role of the doping of the amorphous film precursors, with n-type doping enhancing growth and crystallization, while p-type doping negatively affects NW formation. Key findings include the significance of maintaining optimal etching time and its effect on NW morphology and uniformity. Overall, the results provide a novel method for efficiently growing Si and Ge NWs, emphasizing the importance of carefully controlling growth conditions.

© 2025 Author(s). All article content, except where otherwise noted, is licensed under a Creative Commons Attribution (CC BY) license (<https://creativecommons.org/licenses/by/4.0/>). <https://doi.org/10.1063/5.0249864>

I. INTRODUCTION

Si and Ge nanowires (NWs) have attracted increasing interest in the fields of nanoelectronics,^{1–3} sensors,^{4,5} and solar cells,^{6,7} and their synthesis methods have become an important research topic. These methods include “top-down” and “bottom-up” approaches. The former commonly utilizes techniques such as e-beam for mask preparation,⁸ chemical etching,⁹ and physical etching.¹⁰ However, the fabrication process is tedious, requiring multiple steps, which may reduce the fabrication yield. Moreover, masks created by electron beam (e-beam) lithography need to undergo physical etching, introducing impurities that can affect the electronic properties of the NWs.

The “bottom-up” main growth methods include vapor-liquid-solid (VLS) process based on chemical vapor deposition (CVD),^{11,12} plasma-enhanced CVD (PECVD),^{13,14} and electron beam evaporation.¹⁵ CVD is a common method for preparing Si NWs, whereby a Si gas source (generally silane) reacts at high temperatures and pressures with a catalyst deposited on a substrate,

forming Si NWs. The advantage of using PECVD lies in its ability to achieve low-temperature growth over large areas and providing better control on NW properties. E-beam evaporation needs to be performed under high vacuum conditions, and it requires relatively expensive electron beam equipment. Exploring new preparation methods is a significant research topic. In the traditional VLS mechanism for preparing Si NWs, depositing a layer of metal catalysts, such as Au, on a substrate facilitates the dissociation of silane at high temperatures, forming an eutectic Au/Si alloy and leading to the growth of Si NWs.¹⁶

In this paper, we introduce a new approach to grow Si and Ge NWs where the Si and Ge atoms required for the growth result from the etching of hydrogenated amorphous Si (a-Si:H), Ge (a-Ge:H), or a-SiGe:H thin films. The control of the etching process and the resulting transport of the reactive species from the reactor walls to the substrate offer new opportunities for achieving original NW morphologies and composition. In this work, we systematically investigate the effect of various process parameters on the growth of NWs. In particular, we study the

28 January 2025 12:20:01

effects of pre-coating materials, pre-coating temperatures, precursor ratio, doping precursors, etching temperatures, inter-electrode distances, radio frequency (RF) plasma powers as well as etching times to control NW morphology and composition. Various investigation techniques including scanning electron microscopy (SEM), transmission electron microscopy (HRTEM), high-angle annular dark-field scanning transmission electron microscopy (HAADF-STEM), and energy dispersive x-ray spectroscopy (EDS) were used to characterize the Si and Ge nanostructures.

II. EXPERIMENTAL DETAILS

The PECVD reactor was pumped down to 3×10^{-4} Pa and its electrodes and walls were coated with amorphous materials at a fixed inter-electrode distance of 30 mm. After coating the reactor electrodes and walls with a-Si:H, a-SiGe:H, or a-Ge:H [Fig. 1(a)], the substrates with Sn catalysts were introduced into the PECVD reactor. Two types of Sn precursors were used, including sputtered SnO₂ thin films and colloid SnO₂ nanoparticles [Fig. 1(b)]. 10 nm SnO₂ thin films were deposited on c-Si wafers via RF magnetron sputtering under an Ar flow rate of 50 SCCM, a pressure of 50 Pa, and a RF power of 50 W for 1 min. Colloid SnO₂ nanoparticles (15% in H₂O) with a nominal diameter of 5 nm (Alfa Aesar, China) were diluted in de-ionized water with 1/300 before utilization.

As far as the pre-coating of the a-Si:H layer is considered, the following deposition conditions were used: SiH₄ flow rate of 2 SCCM diluted in 50 SCCM of H₂ as the carrier gas, pressure of 100 Pa, and RF power of 5 W with a deposition time of 10 min.

The nominal thicknesses of a-Si:H layers deposited at 120 and 200 °C are 90 and 140 nm, respectively. In the case of a-Ge:H pre-coating, 50 SCCM of GeH₄ (1% of dilution in H₂) was introduced with a chamber pressure, RF power, and deposition time to be 40 Pa, 5 W, and 2 min, respectively. The nominal thicknesses of a-Ge:H layers deposited at 120 and 200 °C are 15 and 25 nm, respectively.

The etching of amorphous Si thin films typically utilizes gases such as H₂, which can react on their surface, hence achieving an efficient etching effect.^{17,18} The H₂ plasma etching conditions were as follows. H₂ flow rate: 100 SCCM, chamber pressure: 130 Pa and RF power: 100 W. Two series of chamber pre-coating temperature and H₂ etching temperature were applied as shown in Table I. The etching of the a-Si:H layers produces SiH₄ which can be subsequently dissociated by the plasma forming radicals. This process allows us to transport the silicon atoms from the walls of the reactor to the substrate where they react with the catalyst and lead to the growth of NWs. By changing the process parameters, we could determine conditions favoring the growth of NWs. The shape and structure of NWs were investigated with a Hitachi SU-70 scanning electron microscope (SEM). Moreover, TEM lamellas were prepared in a focused ion beam (FIB)-SEM dual beam platform. A Titan Themis electron microscope from Thermo Fisher Scientific (Waltham, MA, USA) was employed for morphological and structural analyses. Operating at 200 kV, this microscope is equipped with a Cs aberration probe corrector for enhanced image resolution and a Super X detector capable of nanoscale chemical analysis for both light and heavy elements.

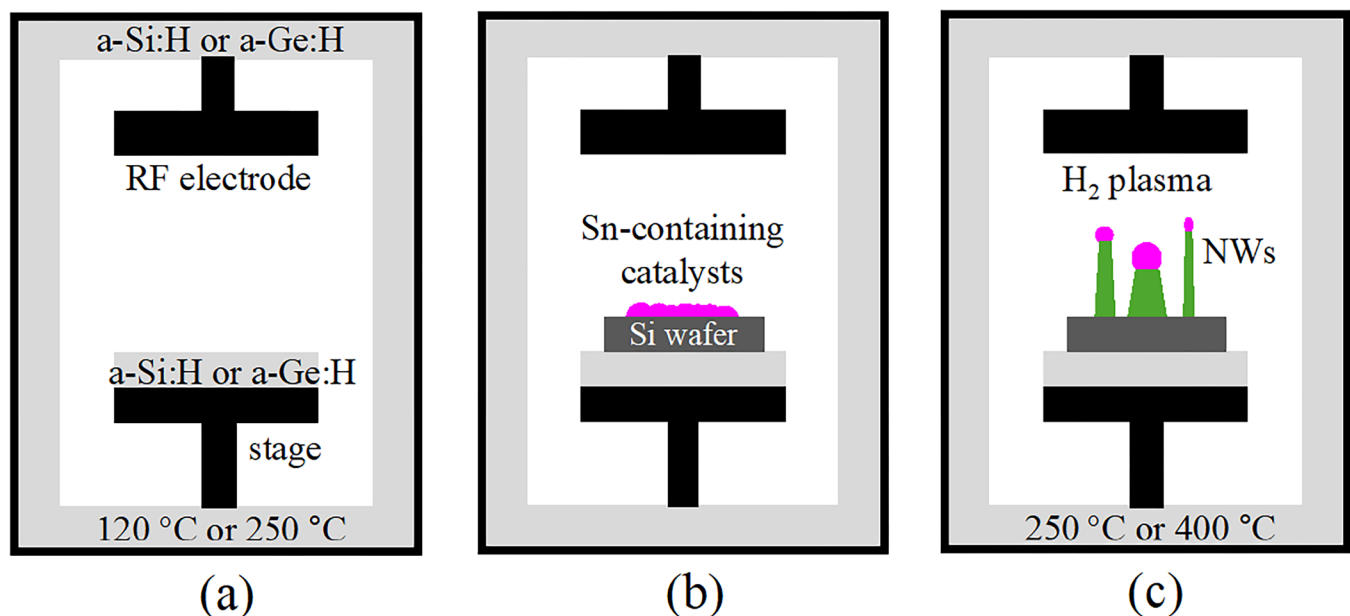


FIG. 1. Schematic illustration of a PECVD reactor. (a) Pre-coating of the reactor with a-Si:H or a-Ge:H layers. (b) Load the Sn-containing catalysts Si wafer into the PECVD reactor. (c) Ignition of the H₂ plasma to produce NWs.

TABLE I. Dependence of NW growth results on pre-coating materials (a-Si:H and a-Ge:H) with two values of chamber pre-coating temperature and H₂ etching temperature. Both the deposition and etching time are 10 min.

Temperature (°C)	a-Si:H			a-Ge:H		
Pre-coating	120	250	250	120	250	250
Etching	250	250	400	250	250	400
NWs	No growth	No growth	Growth	Growth	No growth	No growth

III. RESULTS AND DISCUSSION

Within the context of PECVD, a hydrogen plasma is known to be able to etch the amorphous films deposited on the electrodes and walls of the reactor.¹⁹ Two settings for the substrate temperature were considered for the growth of nanostructures: the pre-coating temperature and the H₂ plasma etching temperature. We choose two values for the etching temperature (250 and 400 °C) which are above the eutectic point temperature of 232 °C, while the pre-coating temperature was fixed at 120 or 250 °C as summarized in Table I.

First of all, let us consider the NW growth at the etching temperature of 400 °C. To be noted here that in this case, only SnO₂ thin films were effective for NW growth. As shown in Table II, we investigated the effects of different parameters on the formation of nanostructures. The conditions for pre-coating and H₂ plasma etching are kept the same as those mentioned above, except for the changes in the parameters corresponding to Table II. The deposition and etching conditions are presented in the experimental part. Section I in Table II reports on the effect of SiH₄ and GeH₄ flow rate ratio. Section (I)(a) shows the SEM images of the substrate after being exposed to the H₂ plasma at 400 °C with the reactor walls coated with a-Ge:H. It can be observed that under these conditions, no NW was grown. In Sec. (I)(b), when the ratio of GeH₄ to SiH₄ was 1.7/0.3 during pre-coating, noticeable changes occurred in the catalyst particles which became smaller and increased in number. In Sec. (I) (c), at a pre-coating ratio of GeH₄ to SiH₄ of 1.5/0.5, several NWs appeared around the catalyst particles. In Sec. (I) (d), when the ratio during pre-coating was 1/1, NWs could be observed, and compared to Sec. (I) (c), both the density and length of the NWs had increased. To further increase the density and length of the NWs, the ratio of GeH₄ to SiH₄ was changed to 0.5/1.5. As shown in Sec. (I) (e), this ratio led to a higher density, yet smaller diameter NWs compared to those in Sec. (I) (d). Finally, in Sec. (I) (f), when the ratio of GeH₄ to SiH₄ during pre-coating was reduced to 0/2 (no addition of GeH₄), thicker but less dense Si NWs were obtained.

In Sec. (II) of Table II we address the effect of adding dopant gases to the reactor wall coating process. Section (II) (a) reveals the surface morphology formed after etching when SiH₄ and B₂H₆ were introduced at a ratio of 2:9 during pre-coating, showing that the catalyst remains unchanged and no NW growth is observed, suggesting that probably no etching occurred under these conditions. Note that B₂H₆ was diluted at 1% in H₂. Section (II) (b)

presents the surface morphology after etching when SiH₄ and PH₃ were introduced at a ratio of 2/9 during pre-coating (PH₃ was diluted at 1% in H₂). In this case NWs have formed, suggesting that n-type a-Si:H film precursor may have a promoting effect on etching of a-Si:H. Therefore, based on this observation, PH₃ was also introduced to see if n-type doping could help in promoting NW growth for a GeH₄ to SiH₄ ratio of 1.5/0.5. Section (II) (c) shows the surface morphology after etching when a mixture of GeH₄, PH₃, and SiH₄ at a ratio of 1.5/9/0.5 was used for pre-coating, resulting in the formation of a considerable number and dense distribution of NWs. Therefore, the addition of PH₃ (n-type doping) proved to have a positive impact on etching and subsequent NW growth. To further study the beneficial effect of PH₃, the experiment shown in Sec. (II) (d) was conducted without introducing SiH₄, i.e., only GeH₄ and PH₃, in order to observe if n-type doping of the a-Ge:H layer could favor the growth of Ge NWs. Section (II) (d) depicts the surface morphology when GeH₄ and PH₃ are used for pre-coating at a ratio of 2/9, where NWs are seen, indicating that indeed PH₃ can promote the growth of not only Si but also Ge NWs at 400 °C.

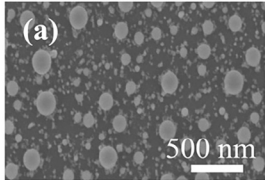
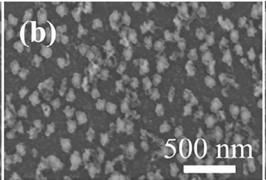
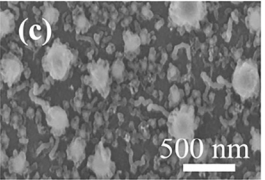
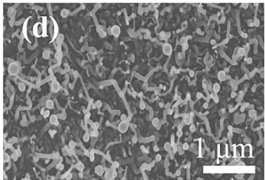
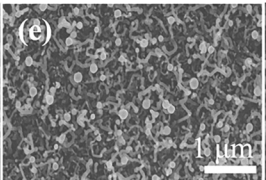
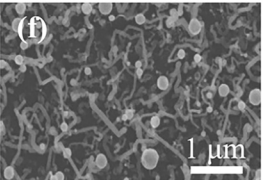
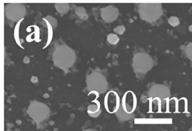
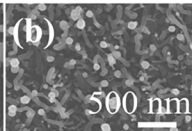
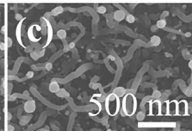
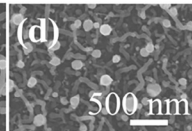
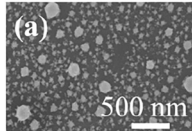
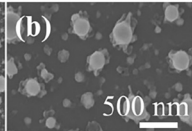
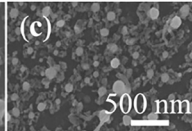
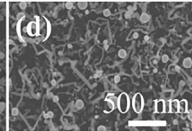
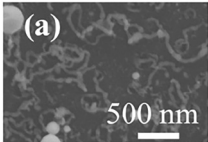
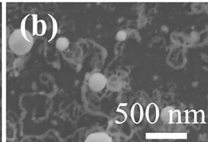
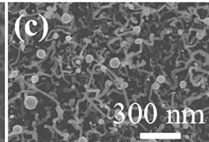
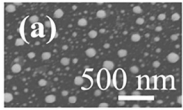
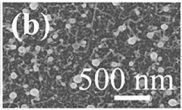
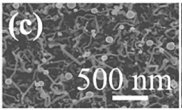
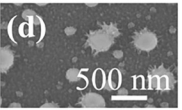
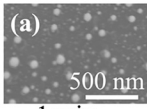
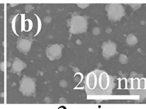
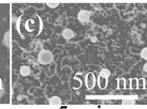
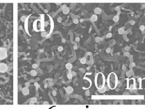
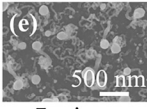
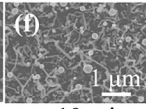

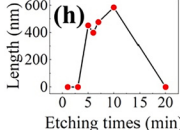
In Sec. III of Table II we present the effect of the substrate temperature during the a-Si:H etching process on NW growth. Section (III) (a) in Table II displays the surface morphology for a substrate temperature of 250 °C, indicating that the catalyst remains mostly unchanged. To further investigate the influence of etching temperature, we raised it to 300 °C. Section (III) (b) shows the surface morphology of the sample at the etching temperature of 300 °C, where small catalyst particles can be seen aggregating into larger ones. Section (III) (c) presents the surface morphology of the sample with the etching temperature further increased to 350 °C. At this temperature, a small number of NWs form, but their quantity remains quite small. Therefore, we increased the substrate temperature to 400 °C, for which a substantial number of NWs are visible.

The distance between the electrodes significantly influences the growth of Si NWs. The surface morphology of the sample for an inter-electrode distance of 70 mm is shown in Sec. (IV) (a), displaying only a few NWs while most areas lack NW growth and even some catalysts remain unchanged. Then, we reduced the inter-electrode distance to 50 mm as shown in Sec. (IV) (b), for which one can see that the density of NWs did increase a bit as compared to 70 mm, but their morphology was poor. Thus, we further decreased the inter-electrode distance to 30 mm, in which case the density of NWs significantly increased, with each catalyst leading to NW growth.

The RF power used during etching is another crucial parameter. Section (V) (a) shows the surface morphology of the substrate after having been exposed to a hydrogen plasma under an RF power of 25 W, where no change in the catalyst can be seen. We thus increased the RF power to 50 W as shown in Sec. (V) (b), under which conditions NWs started to form, but they are short and with a low density. Thus, we further increased the RF power to 100 W, as presented in Sec. (V) (c). We can see that the NWs were distributed more evenly with increased length and diameter. Finally, we increased the power to 300 W, as shown in Sec. (V) (d), in which case, NWs were very short and thin. One can notice that even the Sn catalyst droplet size decreased indicating etching of the

28 January 2025 12:20:01

TABLE II. SEM images showcase nanostructures developed under various process parameters using sputtered SnO₂ thin films. The following pre-coating and etching conditions were used, except when otherwise indicated in the table. The inter-electrode distance was kept at 30 mm for both pre-coating and NW growth processes. The H₂ plasma etching conditions were as follows. H₂ flow rate: 100 SCCM, chamber pressure: 130 Pa, RF power: 100 W and etching temperature: 400 °C. The following deposition conditions of a-Si:H layers were used including SiH₄: 2 SCCM, H₂: 50 SCCM, pressure: 100 Pa, RF power: 5 W, deposition time: 10 min and temperature: 120 °C.

Parameters	SEM images			
				
	2/0	1.7/0.3	1.5/0.5	
Precursor ratio (GeH ₄ /SiH ₄) (I)				
	1/1	0.5/1.5	0/2	
Doping precursors (II)				
	SiH ₄ /B ₂ H ₆ at 2/9	SiH ₄ /PH ₃ at 2/9	GeH ₄ /SiH ₄ /PH ₃ at 1.5/9/0.5	GeH ₄ /PH ₃ at 2/9
Etching temperatures (III)				
	250 °C	300 °C	350 °C	400 °C
Inter-electrode distances (IV)				
	70 mm	50 mm	30 mm	
RF powers (V)				
	25 W	50 W	100 W	300 W
Etching times (VI)				
	1 min	3 min	5 min	6 min
				
	7 min	10 min	20 min	

28 January 2025 12:20:01

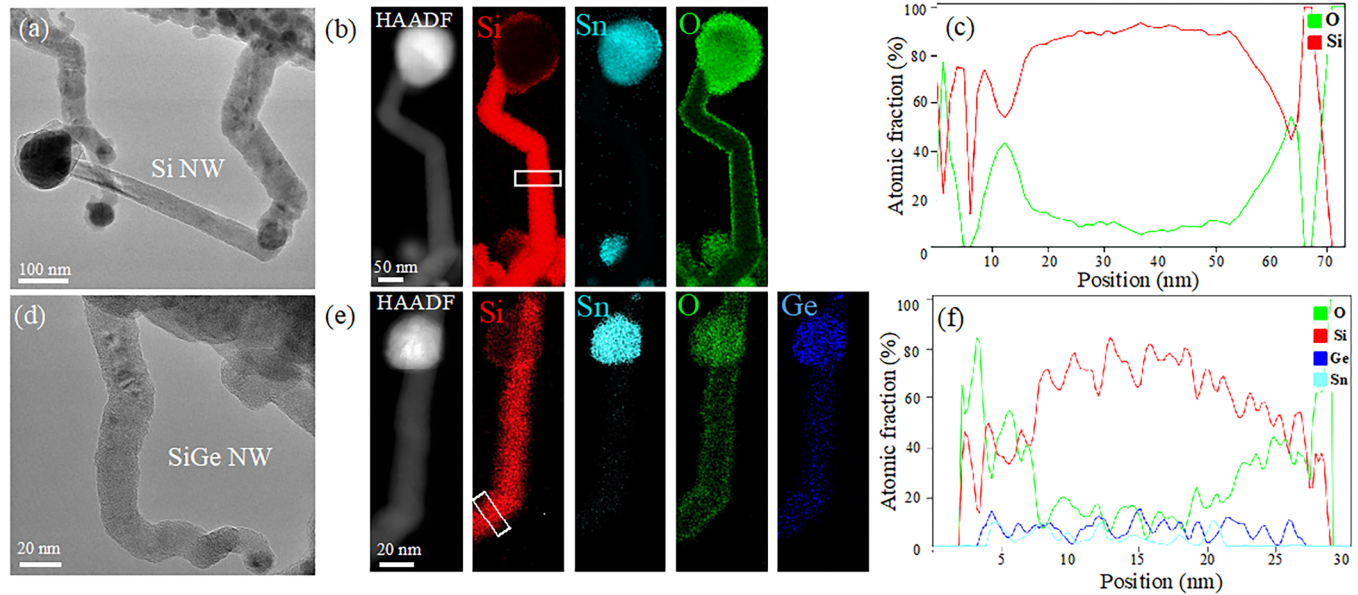


FIG. 2. TEM images of (a) Si NWs and (d) SiGe NWs grown from the sputtered SnO_2 thin films. EDS mapping of (b) Si NWs and (e) SiGe NWs. EDS element profiles of (c) Si NWs and (f) SiGe NWs. The white rectangles in (b) and (e) indicate the locations where the EDS profiles were taken.

Sn at such high-power levels. This is probably because under such RF power and etching time (10 min) we used all the Si available on the walls, so there is only etching at the end of the process, no more chemical transport but eventually a damage of the NWs. Therefore, a RF power of 100 W was chosen as the optimal experimental condition.

The RF power dependence of the NW growth suggests an interplay with the etching time. Thus, determining the optimal process time for NWs is also particularly important. Section (VI) (a) shows the image after an etching time of 1 min, where the reaction has just begun, and the catalysts on the Si wafer surface retain their initial shape. Section (VI) (b) represents the image after an etching time of 3 min where NWs cannot be seen. Section (VI) (c) is the image after an etching time of 5 min, where the NW growth has started, and tiny NWs begin to emerge. We can see in Sec. (VI) (d) that after an etching time of 6 min, the reaction progresses further, and the NWs begin to increase in thickness and length. In Sec. (VI) (e), at an etching time of 7 min, an increase of NW yield occurs, and as the reaction proceeds, in Sec. (VI) (f) at an etching time of 10 min, the NWs' density and dimensions have reached the highest values, with no further increase for longer times, suggesting that a-Si:H from walls has been completely etched and therefore there is no more Si available for NW growth. Indeed, Sec. (VI) (g) corresponding to an etching time of 20 min shows that NWs were no longer present. Section (VI) (h) shows the dependence of NW length on etching time, where the highest NW length at 10 min of etching time can be observed. Note that the average NW growth rate is quite high as 600 nm long wires are obtained after 10 min of growth.

The results in Table II highlight key parameters affecting the etching processes and resulting NW growth. Adding dopant gases,

such as PH_3 , during pre-coating promotes NW formation, as seen in Sec. II, where n-type doping facilitated Si and Ge NW growth. Increasing the substrate temperature in Sec. III shows optimal Si NW formation at 400 °C, while lower temperatures led to limited or no growth. In Sec. IV, reducing the inter-electrode distance to 30 mm enhanced NW density and morphology. Section V demonstrates that RF power of 100 W was optimal, as higher power damaged NWs due to insufficient Si supply. Finally, Sec. VI explores the dependence on etching time, showing NW growth starts after 5 min and peaks at 10 min, where NWs reach their maximum length (~600 nm) and density before depletion of the Si source. These results collectively emphasize the interplay between doping of the thin film precursor, temperature, electrode spacing, RF power, and etching time for controlled and efficient NW growth.

N-type doping of the amorphous film precursor has been found to promote NW growth. This can be explained by the fact that the diffusion in n-type silicon is inhibited compared to the case of a p-type film. As a consequence, there is more hydrogen available at the surface of n-type a-Si:H to promote etching. Moreover, n-type doping of the film precursor may lead to the incorporation of phosphorus into the NWs, facilitating the growth of n-type Si and Ge NWs. B_2H_6 is typically used to introduce p-type doping in Si NWs. However, in our studies, no NWs were formed when the a-Si:H precursor was p-type, which can be explained by a lower etching rate of p-type a-Si:H.²⁰

RF power is essential for initiating and sustaining the etching process. Higher RF powers (100 W) lead to uniform and dense NW growth, but excessive power (300 W) can deplete available materials, resulting in short and thin NWs. In the case of low RF power (25 W), no significant NW growth occurs because the plasma energy is insufficient to efficiently etch the layer from the

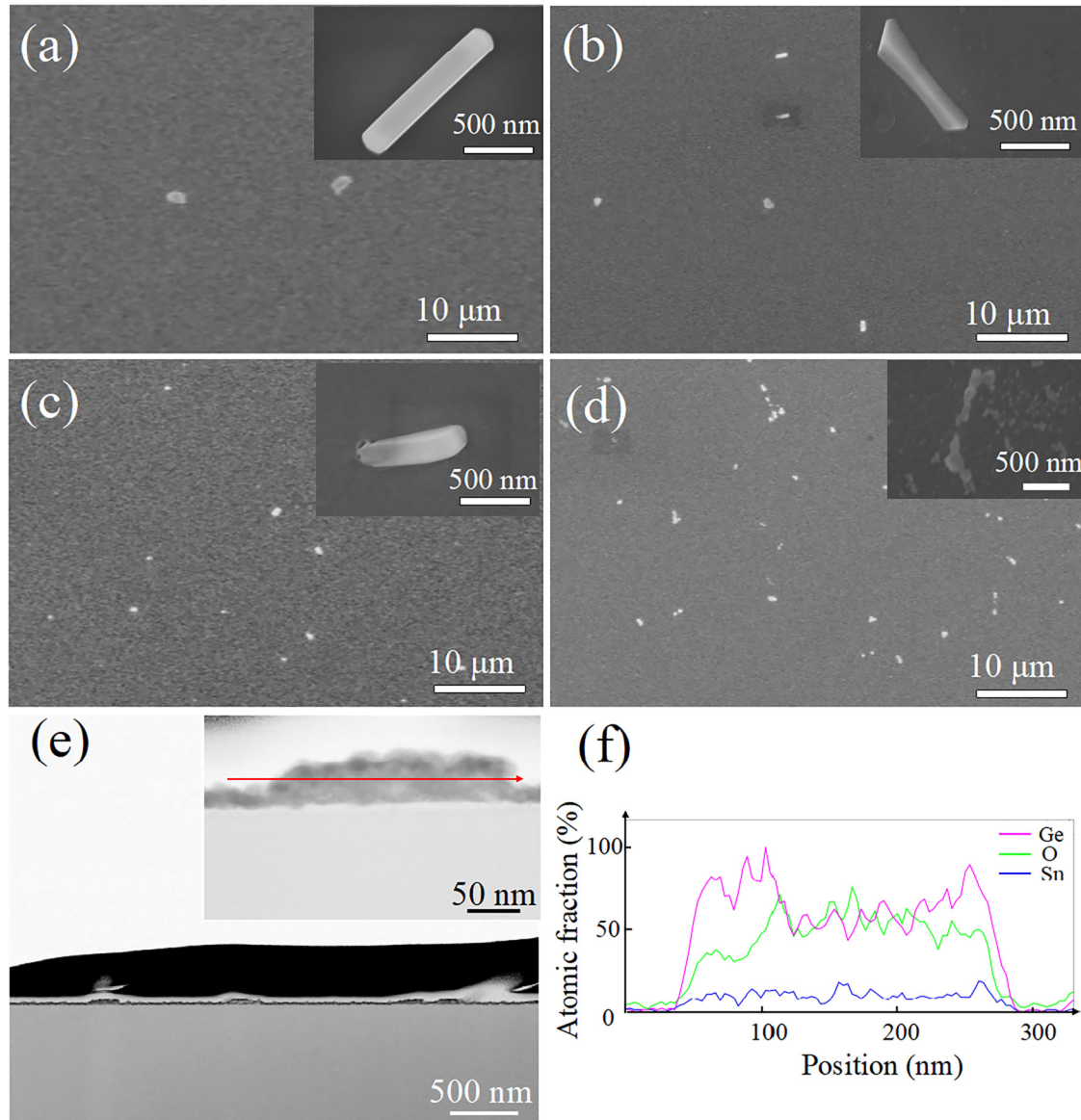


FIG. 3. SEM images of Ge nanostructures grown from colloid SnO_2 nanoparticles at different H_2 plasma etching powers and times. (a) 50 W, 5 min; (b) 100 W, 5 min; (c) 200 W, 5 min, and (d) 100 W; 30 min. (e) Cross-sectional view TEM images of Ge nanostructures grown from colloid SnO_2 nanoparticles at a low etching temperatures (250°C). The inset image shows an enlarged view, with the red arrow indicating the EDS element profile. (f) EDS atom profile (Ge, O, and Sn) in the Ge nanostructures.

walls and fails to provide sufficient Si or Ge atom precursors for NW growth. When the moderate RF Power (100 W) is applied, it produces well-defined, uniform NWs with optimal length and diameter. The plasma power at this level facilitates steady etching and material deposition, creating structured and crystalline NWs. When the RF power is increased to 300 W, it leads to the formation of shorter and thinner NWs. Indeed, excessive power increases the etching rate and leads to the exhaust of the a-Si:H pre-coated on the walls of the reactor, limiting the length and quality of the NWs.

The etching time and RF power determine the length and yield of the NWs. In the case of short etching times (1–3 min), we observe incomplete growth with only small or initial spiky features corresponding to the early stages of NWs growth. The catalysts remain mostly inactive, resulting in incomplete structures. Moderate etching times (5–10 min) produce longer and denser NWs. Their structure becomes more well-defined as the reaction progresses, and NWs grow in length and diameter. When the etching times are prolonged above 20 min it results in the complete

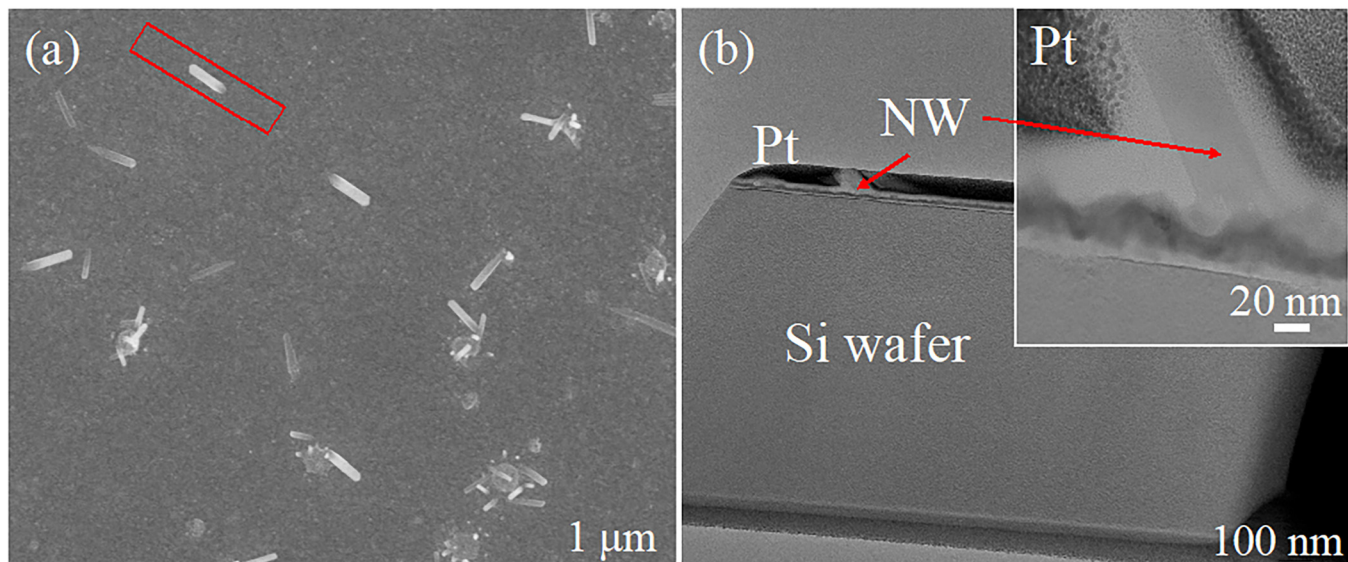


FIG. 4. (a) Top-view SEM image of Ge NWs grown with a sputtered SnO_2 thin film pre-treated with sulfuric acid for 10 min at a low etching temperature (250°C). The red rectangle illustrates where the TEM lamella of NW was prepared. (b) Cross-sectional view of a TEM lamella consisting of Ge NWs from (a). The corresponding enlarged view is presented in the inset.

exhaustion of the material precoated on the walls of the reactor (Si or Ge), causing NWs to stop growing or being damaged and etched away.

To examine the specific morphology and structure of Si NWs, TEM, HAADF-STEM, and EDS were applied. Figure 2(a) shows kinked Si NWs having a small amount of catalyst residue, suggesting that during the NW growth part of the catalyst might detach or rather fall from the tip of the NW and alter the NW's growth direction. The HAADF-STEM and atom mappings of Si, Sn, and O atoms from another NW are presented in Fig. 2(b) where one can see that the NW is made of silicon with an oxide shell resulting from the exposure of the NW to ambient air. The surface morphology of SiGe NWs was also characterized by TEM. Figure 2(d) shows that compared to Si NWs, SiGe NWs are shorter and smaller in diameter. To study the composition of SiGe NWs, we performed HAADF-STEM and EDS mapping from another NW as shown in Fig. 2(e). It reveals that O atoms are mainly located on the outer surface of the catalyst and NWs, Sn atoms are present in the catalyst, Ge atoms are distributed in both the catalyst and the NWs, and Si atoms are primarily found in the main body of the NWs. The corresponding EDS element profiles in Si and SiGe NWs are presented in Figs. 2(c) and 2(f), respectively. The Ge concentration in the SiGe NW is measured to be around 10%.

As presented in Table I, undoped Ge NWs or nanostructures could not be produced at 400°C but can be grown at a lower etching temperature of 250°C . The pre-coating conditions of a-Ge: H were described in the experimental part. In the following parts, let us consider the NW growth with the etching temperature of 250°C . Noted here that in the case, only colloid SnO_2 nanoparticles and SnO_2 thin films pre-treated with sulfuric acid for 10 min did produce NWs. The H_2 plasma etching time and RF power were

varied while keeping other parameters the same as described in the experimental part. As shown in Fig. 3, a 50 W RF plasma power activates few NWs, and higher power leads to higher activation rate of catalyst. Moreover, with the increase of plasma power, the density of NWs increases significantly, but their morphology changes. As shown in Fig. 3(d) the morphology of the produced nanostructures has lost its NW form, indicating that the etching time of 30 min was too long and resulted in the exhaust of the Ge atoms from the reactor wall. Figure 3(e) presents a cross-sectional view of a TEM lamella consisting of in-plane Ge nanostructures from Fig. 3(c) with the corresponding enlarged view shown in the inset. The EDS element profile is shown in Fig. 3(f) indicating the presence of Ge, Sn, and O atoms in Ge nanostructures. The Sn content in Ge nanostructures can be measured to be around 13% at.

Interestingly, out-of-plane Ge NWs can be obtained once the catalyst is changed from colloid SnO_2 nanoparticles to a SnO_2 thin film. Their top-view SEM image is presented in Fig. 4(a). The corresponding TEM lamella shown in Fig. 4(b) confirms that these Ge NWs grow out-of-plane.

These results highlight the critical role of temperature on NW growth. This knowledge allows us to tailor the temperature for specific NW material requirements. The influence of $\text{SiH}_4/\text{GeH}_4$ gas flow rate ratios on NW growth is intriguing. The optimal $\text{GeH}_4/\text{SiH}_4$ ratio of 0.5/1.5 ensures sufficient Si supply for NW formation while limiting Ge incorporation. Co-doping with PH_3 during pre-coating emerges as a key factor for enabling Ge NW growth. Optimizing inter-electrode distance, etching power, and etching time is crucial for successful NW growth. Etching power influences the NW growth rate, while etching time determines the final NW length. Indeed, NW growth relies on the H_2 plasma

28 January 2025 12:20:01

reacting with the surface of amorphous Si films, mainly due to the reactivity of H and H_3^+ ions.²¹ During the reaction, these species combine with Si atoms on the amorphous Si surface, mainly forming SiH_4 reaction products, leading to the etching of the amorphous Si film surface. As the etching time progresses, the reaction for etching of Si atoms from walls and growing of NWs advances further. However, further increasing the etching time, the NWs are completely etched away because of the exhaust of Si or Ge atoms from the reactor walls.

We found that Si NW growth requires a higher etching temperature (400 °C) than Ge NWs (250 °C). This is likely due to the higher bond energy of Si-H (3.29 eV),²² necessitating a higher temperature to facilitate the reaction with a fixed plasma etching power density. In contrast, Ge-H has a lower bond energy (2.99 eV),²² allowing NWs to form at 250 °C. Once the precursor atoms (Si or Ge) are etched successfully from the reactor walls, the corresponding supersaturation in the eutectic droplets is the determining factor for NWs growth. Note that the supersaturation increases with the temperature.²³ As a consequence, more precursor atoms are needed to reach the supersaturation once the temperature is increased. Moreover, the etching rate of amorphous a-Si:H or a-Ge:H inversely depends on the temperature.^{18,24} Lower etching temperature favors the production of precursor atoms. Therefore, Ge NWs can be produced at the low temperature of 250 °C instead of 400 °C.

The diameter and length of NWs are heavily influenced by precursor gas ratios, RF power, and etching time. Higher SiH_4 ratios, moderate RF power, and optimal etching times lead to thicker and longer NWs. The density of NWs can be enhanced by higher RF power, shorter inter-electrode distance, and n-type doping of the film precursor. Interestingly, the density of Ge NWs is significantly lower than Si NWs. At a lower temperature (250 °C), Ge NWs can grow but with smaller, thinner, and less dense NWs. Si NW growth is hindered at these temperatures. Moderate temperatures (e.g., 400 °C) are better suited for Si NW growth.

IV. CONCLUSIONS

This work presents a novel method for growing Si or Ge NWs, where Si wafers coated with Sn-containing catalysts were loaded into a PECVD reactor coated with undoped or doped a-Si:H, a-SiGe:H, or a-Ge:H layers, followed by etching with H_2 to promote chemical transport and growth of NWs. Throughout the experiments, we found that variations in process parameters, especially the substrate temperature, have a strong impact on the results, leading to the following conclusions. Combining the pre-coating temperature of 250 °C with the plasma etching of 400 °C is beneficial to produce Si NWs. Pre-coating the walls of the reactor with a-Si:H promotes the growth of NWs, while a-Ge:H inhibits it. In the case of a-SiGe:H pre-coating the optimal ratio of GeH_4/SiH_4 is 0.5/1.5. Interestingly, using a n-type a-Ge:H precursor can lead to the growth of Ge NWs even at 400 °C. NWs start to grow only when a certain inter-electrode distance, etching temperature, and power are applied, typically choosing a 30 mm inter-electrode distance, a 400 °C etching temperature, and 100 W RF power. Lowering the pre-coating temperature to 120 °C and the plasma etching temperature to 250 °C is helpful to fabricate Ge NWs.

ACKNOWLEDGMENTS

W.C. was supported the Zhejiang Provincial Natural Science Foundation of China (Grant No. LY24F040001). TEM and EDS characterizations were performed in the frame of the French Government program of investment for the future (Programme d'Investissement d'Avenir—ANR-IEED-002-01 and TEMPOS Equipex—ANR-10-EQPX-50, pole NanoTEM).

AUTHOR DECLARATIONS

Conflict of Interest

The authors have no conflicts to disclose.

Author Contributions

Ke Yang: Investigation (equal); Writing – original draft (equal); Writing – review & editing (equal). **Xianjun Zhu:** Investigation (equal); Writing – original draft (equal); Writing – review & editing (equal). **Ruiling Gong:** Investigation (equal); Writing – review & editing (equal). **Ileana Florea:** Investigation (equal); Writing – original draft (equal); Writing – review & editing (equal). **Pere Roca i Cabarrocas:** Writing – original draft (equal); Writing – review & editing (equal). **Wanghua Chen:** Funding acquisition (equal); Investigation (equal); Writing – original draft (equal); Writing – review & editing (equal).

DATA AVAILABILITY

The data that support the findings of this study are available within the article.

REFERENCES

- ¹S. Gao, S. Hong, S. Park, H. Y. Jung, W. Liang, Y. Lee, C. W. Ahn, J. Y. Byun, J. Seo, M. G. Hahm, H. Kim, K. Kim, Y. Yi, H. Wang, M. Upmanyu, S.-G. Lee, Y. Homma, H. Terrones, and Y. J. Jung, *Nat. Commun.* **13**, 3467 (2022).
- ²T. S. Teitsworth, D. J. Hill, S. R. Litvin, E. T. Ritchie, J.-S. Park, J. P. Custer, A. D. Taggart, S. R. Bottum, S. E. Morley, S. Kim, J. R. McBride, J. M. Atkin, and J. F. Cahoon, *Nature* **614**, 270 (2023).
- ³F. A. Nuñez-Murillo and J. R. Cárdenas, *J. Appl. Phys.* **134**, 214302 (2023).
- ⁴C. Yang, W. Liao, J. Wang, and L. Yu, *ACS Sens.* **9**, 6284 (2024).
- ⁵I. Zeimpekis, T. Rahman, O. M. Leung, J. Tyson, M. Ebert, S. A. Boden, C. Ponce De Leon, and K. A. Morgan, *ACS Appl. Energy Mater.* **7**, 2299 (2024).
- ⁶W. Chen and P. Roca i Cabarrocas, *Nanotechnology* **30**, 194002 (2019).
- ⁷A. Khaled, M. F. O. Hameed, B. M. A. Rahman, K. T. V. Grattan, S. S. A. Obayya, and M. Hussein, *Opt. Express* **28**, 31020 (2020).
- ⁸S. Mukherjee, M. Y. Elsayed, H. H. Tawfik, and M. N. El-Gamal, *Sensors* **24**, 7144 (2024).
- ⁹F. J. Wendisch, M. Rey, N. Vogel, and G. R. Bourret, *Chem. Mater.* **32**, 9425 (2020).
- ¹⁰A. D. Refino, N. Yulianto, I. Syamsu, A. P. Nugroho, N. H. Hawari, A. Syring, E. Kartini, F. Iskandar, T. Voss, A. Sumboja, E. Peiner, and H. S. Wasisto, *Sci. Rep.* **11**, 19779 (2021).
- ¹¹R. A. Puglisi, C. Bongiorno, S. Caccamo, E. Fazio, G. Mannino, F. Neri, S. Scalesi, D. Spucches, and A. La Magna, *ACS Omega* **4**, 17967 (2019).
- ¹²W. Chen, V. G. Dubrovskii, X. Liu, T. Xu, R. Larde, J. P. Nys, B. Grandidier, D. Stievenard, G. Patriarche, and P. Pareige, *J. Appl. Phys.* **111**, 094909 (2012).
- ¹³Z. Xue, W. Chen, X. Meng, J. Xu, Y. Shi, K. Chen, L. Yu, and P. Roca i Cabarrocas, *Appl. Surf. Sci.* **593**, 153435 (2022).

- ¹⁴W. Wang, É Ngo, P. Bulkin, Z. Zhang, M. Foldyna, P. Roca i Cabarrocas, E. V. Johnson, and J.-L. Maurice, *Nanomaterials* **13**, 2061 (2023).
- ¹⁵R. Rakesh Kumar, K. Narasimha Rao, and A. R. Phani, *Appl. Nanosci.* **1**, 211 (2011).
- ¹⁶R. S. Wagner and W. C. Ellis, *Appl. Phys. Lett.* **4**, 89 (1964).
- ¹⁷S. Vepřek and F.-A. Sarott, *Plasma Chem. Plasma Process.* **2**, 233 (1982).
- ¹⁸A. Fontcuberta i Morral and P. Roca i Cabarrocas, *J. Non-Cryst. Solids* **299–302**, 196 (2002).
- ¹⁹F. Kail, A. Fontcuberta i Morral, A. Hadjadj, P. Roca i Cabarrocas, and A. Beorchia, *Philos. Mag.* **84**, 595 (2004).
- ²⁰A. Hadjadj, N. Pham, P. Roca i Cabarrocas, and O. Jbara, *Appl. Phys. Lett.* **94**, 061909 (2009).
- ²¹T. Zhang, J.-M. Orlac'h, M. Ghosh, V. Giovangigli, P. Roca i Cabarrocas, and T. Novikova, *Plasma Sour. Sci. Technol.* **30**, 075024 (2021).
- ²²M. Daouahi, A. Ben Othmane, K. Zellama, A. Zeinert, M. Essamet, and H. Bouchriha, *Solid State Commun.* **120**, 243 (2001).
- ²³S. Paiman, Q. Gao, H. J. Joyce, Y. Kim, H. H. Tan, C. Jagadish, X. Zhang, Y. Guo, and J. Zou, *J. Phys. D: Appl. Phys.* **43**, 445402 (2010).
- ²⁴S. P. Hong, J. Kim, J.-B. Park, K. S. Oh, Y.-W. Kim, S. J. Yoo, and D. C. Kim, *Thin Solid Films* **579**, 127 (2015).